IOPscience iopscience.iop.org

Home Search Collections Journals About Contact us My IOPscience

Layered growth modelling of epitaxial growth processes for SiC polytypes

This article has been downloaded from IOPscience. Please scroll down to see the full text article.

2005 J. Phys.: Condens. Matter 17 5355

(http://iopscience.iop.org/0953-8984/17/35/004)

View the table of contents for this issue, or go to the journal homepage for more

Download details:
IP Address: 129.252.86.83
The article was downloaded on 28/05/2010 at 05:53

Please note that terms and conditions apply.

INSTITUTE OF PHYSICS PUBLISHING JOURNAL OF PHYSICS: CONDENSED MATTER

J. Phys.: Condens. Matter **17** (2005) 5355–5366 doi:10.1088/0953-8984/17/35/004

Layered growth modelling of epitaxial growth processes for SiC polytypes

Zhaoqing Liu and Jun Ni

Department of Physics and Key Laboratory of Atomic and Molecular Nanoscience (Ministry of Education), Tsinghua University, Beijing 100084, People's Republic of China

E-mail: junni@mail.tsinghua.edu.cn

Received 14 March 2005, in final form 2 August 2005
Published 19 August 2005
Online at stacks.iop.org/JPhysCM/17/5355

Abstract
Epitaxial growth processes for SiC polytypes in which a SiC substrate is employed are studied using a layered growth model. The corresponding phase diagrams of epitaxial growth processes are given. First-principles calculations are used to determine the parameters in the layered growth model. The layered growth phase diagrams show that when the rearrangement of atoms in one surface Si–C bilayer is allowed, the 3C-SiC structure is formed. When the rearrangement of atoms in two surface Si–C bilayers is allowed, the 4H-SiC structure is formed. When the rearrangement of atoms in more than two surface Si–C bilayers, excepting the case of five surface Si–C bilayers, is allowed, the 6H-SiC structure is formed, which is also shown to be the ground state structure. When the rearrangement of atoms in five surface Si–C bilayers is allowed, the 15R-SiC structure is formed. Thus the 3C-SiC phase would grow epitaxially at low temperature, the 4H-SiC phase would grow epitaxially at intermediate temperature and the 6H-SiC or 15R-SiC phases would grow epitaxially at higher temperature.

(Some figures in this article are in colour only in the electronic version)

1. Introduction

Silicon carbide (SiC) has several advantages over other semiconductors such as Si and GaAs in its wide band gap, high thermal conductivity, high carrier mobility, high electric field breakdown strength, radiation resistance and chemical stability, which makes it one of the most attractive materials for devices used in high-temperature, high-pressure, high-frequency and high-radiation environments [1].

Silicon carbide (SiC) exhibits the most pronounced polytypism as the only known naturally stable group IV compound. More than 200 SiC polytypes have been determined to date [2]. The most common polytypes are zinc-blende SiC (3C-SiC in Ramsdell notation), wurtzite SiC (2H-SiC in Ramsdell notation), 4H-SiC, 6H-SiC and 15R-SiC. All the SiC polytypes could

be considered as different arrangements of cubic or hexagonal Si–C bilayers, stacking along the cubic [111] or the equivalent hexagonal [0001] direction geometrically. 3C-SiC is pure cubic stacking of Si–C bilayers in the [111] direction and 2H-SiC is pure hexagonal stacking of Si–C bilayers in the [0001] direction. The other polytypes in the Ramsdell notation, *n*H-SiC (hexagonal) or *n*R-SiC (rhombohedral), can be considered as combinations of these two stacking sequences with *n* Si–C bilayers in the primitive cell—such as 4H-SiC and 6H-SiC with four and six Si–C bilayers in the corresponding hexagonal unit cell. These polytypes lie very close together in energy and possess similar lattice constants.

The origin of polytypism in SiC is still not completely understood though it has been studied for many years. To understand the polytypism in SiC theoretically, it is important to examine the structural and thermal properties of the SiC polytypes using the first-principles approach. Whether the polytypes should be viewed as non-equilibrium structures arising from special growth mechanisms or stable (possibly metastable) thermodynamic phases with a specific stability range of external parameters (such as pressure and temperature) has long been debated. When a thermodynamic approach to the problem is used, the most important quantities are the total energy differences between the various SiC polytypes at zero kelvins. Several groups have used a first-principles approach to calculate these energy differences and given some important explanations of various properties of SiC [3–11]. However, there are some significant discrepancies between the results of the various first-principles calculations. Furthermore, several calculated results appear to invalidate some of the important conclusions drawn by Heine *et al* [12–14]. The phenomenon of polytypism has also been related to the phonon, which may stabilize the polytypism with its contributions to the free energy. So vibrational entropies of these SiC polytypes at higher temperatures have also been discussed by Heine *et al* [13–15], Zywietz *et al* [16] and Bechstedt *et al* [11]. Much experimental knowledge on the growth and formation of SiC polytypes has been obtained over the last 40 years. Factors affecting the crystal are the temperature and the pressure in the growth chamber, the polarity of the seed crystal, the substrate orientations, the presence of certain impurities, the Si/C ratio and the lattice mismatch with the substrate. In the case of a film with lattice mismatch, the first few monolayers will try to minimize the strain due to a given lattice mismatch with the substrate. This effect may allow the growth of phases (metastable phases, or polytypes) that would not grow without lattice mismatch. Additionally, the variety of surface superstructures changing the surface energy plays a role in the epitaxial growth process [17]. Recently, Fissel *et al* succeeded in the realization of SiC polytype heterostructures like 4H/3C/4H by careful control of the surface superstructure and the thermodynamic conditions during MBE growth [18, 19]. Off-oriented (vicinal-oriented) and on-oriented (well-oriented) SiC substrates are both employed for SiC crystal growth. SiC growth on off-axis SiC substrates is known as ‘step-controlled epitaxy’ in which grown layers inherit the stacking order of the substrates through a step-flow growth, thereby preserving the polytype of the substrates. So the polytypes obtained through ‘step-controlled epitaxy’ are limited by the substrates. Such step-flow growth is widely used to grow high-quality 4H- and 6H-SiC at reduced temperatures on off-axis 4H- and 6H-SiC substrates [20–22]. Much of the SiC growth is done on on-axis SiC substrates; with this approach the polytype may be different from that of the substrate [23–32] and the films should be grown on well-oriented surfaces because of the frequent occurrence of double positioning boundaries (DPBs) in films grown on vicinal surfaces [29]. In our model, we focus on the on-oriented (well-oriented) SiC growth and do not discuss ‘step-controlled epitaxy’.

Different first-principles calculations all obtain that the 3C-SiC phase is much higher in energy than the 4H-SiC and 6H-SiC phases at zero kelvins [3–10], and theoretical studies also show that the 3C-SiC phase has a higher phonon free energy [15]. These results seem to suggest that the 3C-SiC phase is never the stable structure at any temperature. However

experiments [2, 33–36] found that the 3C-SiC phase does prefer to grow epitaxially. A good model that Heine *et al* [12] have introduced can explain the experimental phenomenon. For the layered polytypic structure of SiC, growth is considered to be a layer-by-layer process, adding one Si–C bilayer at a time to the growing crystal, with the rearrangement of atoms in each new surface bilayer being allowed to orient the new surface bilayer into its most energetically favourable stacking orientation, without allowing the atoms in the lower bilayers to rearrange to give a global energy minimum of the growing crystal. The 3C-SiC phase could be explained as a result of epitaxial growth. Thus this model includes some aspects of the growth process, and permits non-equilibrium phases to be formed.

When the temperature is high, one would expect the rearrangement of atoms in more than one surface bilayer to be allowed to orient the surface bilayers into their most energetically favourable stacking orientations. If the rearrangement of atoms in many more bilayers near the surface is allowed, what kinds of structures can be formed? The present work extends the one-layer model to a many-layer one and uses it to explain the growth conditions for other non-equilibrium phases of silicon carbide. We have also performed first-principles calculations for the energy differences of these SiC polytypes. Several distinct conclusions have been drawn, as compared to the previous calculations [3–10].

2. Methods

All the SiC polytypes can be considered as different arrangements of cubic or hexagonal Si–C bilayers with stackings along the cubic [111] or the equivalent hexagonal [0001] direction. This one-dimensional character of the stacking differences suggests the description of the differences in terms of an axial next-nearest neighbour Ising (ANNNI) model [11, 37] in which the total energy of the system per Si–C pair may be represented by

$$E = E_0 - \frac{1}{n}\sum_{i=1}^{n}\sum_{k} J_k \sigma_i \sigma_{i+k} \tag{1}$$

where E_0 is a common energy reference and n is the number of bilayers in the unit cell of the nH-, nR- or nC-SiC polytypes, i.e., $n = 2, 3, 4$ and 6 for 2H-, 3C-, 4H- and 6H-SiC, respectively. A 'spin' $\sigma_i = \pm 1$ is associated with each close-packed Si–C bilayer such that parallel spins represent a locally cubic stacking and antiparallel spins represent a locally hexagonal stacking. The parameters J_k represent the interlayer interaction between two bilayers. More complicated interactions, such as four-spin terms, are neglected. Assuming that the long-range interactions are small, we restrict the interlayer interactions to third neighbours ($k \leqslant 3$). Thus the energy differences of the polytypes can be expressed in terms of the interlayer interaction parameters, i.e.,

$$\begin{aligned}
E_{2H} - E_{3C} &= 2(J_1 + J_3),\\
E_{4H} - E_{3C} &= J_1 + 2J_2 + J_3,\\
E_{6H} - E_{3C} &= \tfrac{2}{3}(J_1 + 2J_2 + 3J_3),\\
E_{8H} - E_{3C} &= \tfrac{1}{2}(J_1 + 2J_2 + 3J_3),\\
E_{10H} - E_{3C} &= \tfrac{2}{5}(J_1 + 2J_2 + 3J_3),\\
E_{9R} - E_{3C} &= \tfrac{4}{3}(J_1 + J_2),\\
E_{15R} - E_{3C} &= \tfrac{4}{5}(J_1 + 2J_2 + 2J_3).
\end{aligned} \tag{2}$$

We have performed the calculations of the SiC polytype energies using VASP (Vienna *ab initio* simulation package) [38]. The approach is based on an iterative solution of the Kohn–Sham equations of density functional theory (DFT) in a plane-wave basis set with the

projector-augmented-wave (PAW) method [39]. The exchange–correlation functional with the generalized gradient approximation (GGA) given by Perdew and Wang [40] is used. We have also used the exchange–correlation functional with the local density approximation (LDA) given by Ceperley and Alder [41] in the parametrization of Perdew and Zunger [42] for comparison. We set the plane-wave cut-off energy to be 800 eV. A mesh of gamma centred grids $11 \times 11 \times 3$ is used to sample the Brillouin zone and the optimizations of the lattice constants and the atom coordinates are made by conjugate gradient minimization of the total energy. The tolerance of the energy convergence is 10^{-5} eV. In order to determine the perfect interlayer interaction parameters J_k in the ANNNI model, we have employed the same size of supercells, containing 24 atoms for all these polytypes. Thus the supercells for 2H-, 3C-, 4H- and 6H-SiC consist of 6, 4, 3 and 2 primitive unit cells for each structure, respectively. It is preferable to employ the same size of supercell for all polytypes containing the same number of atoms rather than the smallest possible unit cell in each case due to the cancellation of systematic errors when the total energies of different polytypes are compared. In such a way, the more accurate crystal *ab initio* lattice constants (obtained by total energy minimization), crystal atomic positions (obtained by intrasupercell atomic relaxation) and J_k parameters in the ANNNI model can be determined.

From the total energies of SiC polytypes, we can elicit the interlayer interaction parameters in the ANNNI model according to the formulations

$$\begin{aligned} J_1 &= (2E_{2H} - E_{3C} + 2E_{4H} - 3E_{6H})/4, \\ J_2 &= -(E_{2H} + E_{3C} - 2E_{4H})/4, \\ J_3 &= -(E_{3C} + 2E_{4H} - 3E_{6H})/4. \end{aligned} \tag{3}$$

Vapour phase epitaxy (VPE) deposition methods are non-equilibrium processes. The structure of SiC formed by such growth processes is not always the lowest-energy structure. As a SiC substrate is commonly used in epitaxial growth process for SiC polytypes, we also employ a SiC substrate in our layered growth model. So our calculations and conclusions apply in cases of zero lattice mismatch. As we restrict the interlayer interactions to third neighbours, the total energies of the ANNNI model for the SiC polytypes are only related to the top three substrate Si–C bilayers, represented by $(\sigma_{i-2}, \sigma_{i-1}, \sigma_i)$. There are 2^3 possible types of combination of the top three substrate Si–C bilayers: $\sigma_{i-2}, \sigma_{i-1}, \sigma_i = \pm 1$. If symmetry is taken into account, only four types of combination are left, i.e., $(\bar{1}\bar{1}\bar{1})$, $(1\bar{1}\bar{1})$, $(\bar{1}1\bar{1})$ and $(\bar{1}\bar{1}1)$. In our layered grown model, when the rearrangement of atoms in one surface Si–C bilayer is allowed to orient the surface Si–C bilayer into its most energetically favourable stacking orientation, the system energy is added, with

$$E_{i+1} = E_0 - \sum_{k=1}^{3} J_k \sigma_{i+1} \sigma_{i+1-k}$$

when a new Si–C bilayer represented as σ_{i+1} grows. We select the value of σ_{i+1} ($\sigma_{i+1} = \pm 1$) which minimizes the additive energy E_{i+1} with fixed σ values of the underlayers (the values of σ_{i-2}, σ_{i-1} and σ_i) and this value of σ_{i+1} is the stacking orientation of the new surface Si–C bilayer (the $(i+1)$th Si–C bilayer). The $(i+1)$th Si–C bilayer is then buried in that stacking orientation by the next Si–C bilayer (the $(i+2)$th Si–C bilayer) without subsequent reorienting, which means that the value of σ_{i+1} is then fixed. In the same way, we select the value of σ_{i+2} which minimizes the additive energy

$$E_{i+2} = E_0 - \sum_{k=1}^{3} J_k \sigma_{i+2} \sigma_{i+2-k}$$

with fixed σ_{i+1} value and those of the lower Si–C bilayers. Then we select the value of σ_{i+3}

which minimizes the additive energy

$$E_{i+3} = E_0 - \sum_{k=1}^{3} J_k \sigma_{i+3} \sigma_{i+3-k}$$

with fixed σ_{i+2} value and those of the lower Si–C bilayers, and so on. In such a way, we simulate the epitaxial growth process when the rearrangement of atoms in one surface Si–C bilayer is allowed. When the rearrangement of atoms in two surface Si–C bilayers is allowed to orient the two surface Si–C bilayers into their most energetically favourable stacking orientations, we should select the values of σ_{i+1} and σ_{i+2} which minimize the sum of energies E_{i+1} and E_{i+2} with fixed σ_i value and those of the lower Si–C bilayers. The values of σ_{i+1} and σ_{i+2} are the stacking orientations of the two surface Si–C bilayers (the $(i + 1)$th and $(i + 2)$th Si–C bilayers). When a subsequent Si–C bilayer (the $(i + 3)$th Si–C bilayer) grows, we select the values of σ_{i+2} and σ_{i+3} minimizing the sum of energies E_{i+2} and E_{i+3} with fixed σ_{i+1} value and those of the lower Si–C bilayers. When a subsequent Si–C bilayer (the $(i + 4)$th Si–C bilayer) grows, we select the values of σ_{i+3} and σ_{i+4} minimizing the sum of energies E_{i+3} and E_{i+4} with fixed σ_{i+2} value and those of the lower Si–C bilayers. In the same way, we select the subsequent values of σ_{i+4} and σ_{i+5}, and so on. In such a way, we simulate the epitaxial growth process when the rearrangement of atoms in two surface Si–C bilayers is allowed. When the rearrangement of atoms in m surface Si–C bilayers is allowed to orient the m surface Si–C bilayers into their most energetically favourable stacking orientations, we should select the values of $\sigma_{i+1}, \sigma_{i+2}, \ldots, \sigma_{i+m}$ which minimize the sum of energies $E_{i+1}, E_{i+2}, \ldots, E_{i+m}$ with fixed σ_i value and those of the lower Si–C bilayers. When the subsequent Si–C bilayer (the $(i + m + 1)$th Si–C bilayer) grows, we select the values of $\sigma_{i+2}, \sigma_{i+3}, \ldots, \sigma_{i+m+1}$ minimizing the sum of energies $E_{i+2}, E_{i+3}, \ldots, E_{i+m+1}$ with fixed σ_{i+1} value and those of the lower Si–C bilayers. When the subsequent Si–C bilayer (the $(i+m+2)$th Si–C bilayer) grows, we select the values of $\sigma_{i+3}, \sigma_{i+4}, \ldots, \sigma_{i+m+2}$ minimizing the sum of energies $E_{i+3}, E_{i+4}, \ldots, E_{i+m+2}$ with fixed σ_{i+2} value and those of the lower Si–C bilayers, and so on. In such a way, we simulate the epitaxial growth process when the rearrangement of atoms in m surface Si–C bilayers is allowed. This model is just a simplification of the growth process, but it is obvious that the layers near the surface would have greater freedom to orient than a layer in the bulk. As the temperature of the epitaxial growth process increases or the anneal process becomes slower, the number of surface Si–C bilayers where the rearrangement of atoms is allowed will increase.

3. Results

We have calculated the hexagonal lattice constants a (basal plane) and c (orthogonal to the basal plane) in ångströms for SiC polytypes in order to validate our first-principles calculations. The values compared to the experimental data are listed in table 1. The lattice constants a for all polytypes are found to be within 1% of the experimental values and the c/na are in good agreement with experiments, with errors within 0.02% relative to the experimental values. Since we relax the structures with respect to volume, cell shape and internal position, our calculated lattice constants have smaller errors to those from previous first-principles calculations [4, 5, 9] relative to the experimental values. Our calculated lattice constants obtained with the DFT-LDA are a little smaller than the experimental values, while those obtained with the DFT-GGA are a little larger than the experimental values, which is in agreement with the general error tendency of the first-principles calculations.

The relative energies of SiC polytypes (meV/SiC pair) with reference to the 3C-SiC phase and the values of the interlayer interaction parameters J_k (meV/SiC pair) are listed in table 2. Our results calculated with the DFT-GGA show that the 6H-SiC phase has the lowest energy,

Table 1. Values of the calculated and experimental hexagonal lattice constants a (basal plane) and c (orthogonal to the basal plane) in Å. The value of c is divided by na; $n = 2$, 3, 4 and 6 for 2H-, 3C-, 4H-and 6H-SiC, respectively.

Lattice constant (Å)		3C-SiC	2H-SiC	4H-SiC	6H-SiC
a	Theory (LDA)	3.061 5	3.057 3	3.059 0	3.059 9
	Theory (GGA)	3.093 8	3.089 0	3.091 0	3.091 9
	Exp. [43]	3.082		3.073	3.080
	Exp. [44]			3.080 51	3.081 29
	Exp. [45]		3.076		
c/na	Theory (LDA)	0.816 50	0.824 05	0.818 40	0.817 82
	Theory (GGA)	0.816 50	0.820 63	0.818 51	0.817 91
	Exp. [43]	0.816 50		0.817 85	0.818 04
	Exp. [44]			0.818 44	0.817 81
	Exp. [45]		0.820 5		

Table 2. Total energies of SiC polytypes (meV/Si–C pair) with reference to 3C-SiC and calculated values of J_k (meV/Si–C pair).

Reference	E_{2H}	E_{4H}	E_{6H}	E_{3C}	J_1	J_2	J_3
[3]	8.70	−0.77	−1.18	0	4.85	−2.56	−0.50
[4]	3.60	−5.00	−3.60	0	2.00	−3.40	−0.20
[5]	1.80	−4.00	−2.91	0	1.08	−2.45	−0.18
[6]	5.16	−4.40	−2.85	0	2.33	−3.49	0.25
[7]	6.00	−2.40	−2.20	0	3.47	−2.71	−0.47
[8]	5.4040	−2.4380	−2.0973	0	3.0560	−2.5700	−0.3540
[9]	4.2668	−2.4784	−2.1801	0	2.5293	−2.3059	−0.3959
Present (LDA)	4.6458	−2.5325	−2.2092	0	2.7135	−2.4277	−0.3906
Present (GGA)	6.7925	−0.6992	−0.9042	0	3.7248	−2.0480	−0.3285

with the total energies of the SiC polytypes in the order $E_{6H} < E_{4H} < E_{3C} < E_{2H}$, while those calculated with the DFT-LDA give the 4H-SiC phase as the lowest-energy structure, with the total energies of the SiC polytypes in the order $E_{4H} < E_{6H} < E_{3C} < E_{2H}$. Comparing our calculated results to those of the previous first-principles calculations [3–9], it can be seen that our result obtained with the DFT-LDA is similar to those of [7–9], and in especially good agreement with those of [9] because they employ supercells containing 24 atoms for all these SiC polytypes, as we do. The computational method employed in [8] is the full-potential linear muffin-tin orbital method with the DFT-GGA, while norm-conserving pseudopotentials with the DFT-LDA are employed in [3–7, 9].

The phase diagram of ground states for the ANNNI model is given in figure 1. We choose the ratios J_3/J_1 and J_2/J_1 as coordinates. In the selected parameter regions, a multiphase (3C, 4H and 6H) degeneracy point appears at $J_3 = 0$ and $J_1 = -2J_2$. The interlayer interaction parameter points obtained from our first-principles calculations are indicated in the phase diagram. Those obtained from the first-principles results of [3–9] are also given, with different symbols, in the phase diagram for comparison. It can be that our result obtained with the DFT-GGA and that of [3] show that the 6H-SiC phase has the lowest energy, while our result obtained with the DFT-LDA and those of [4–9] show that the 4H-SiC phase is the lowest-energy structure. According to Heine [13], the origin of the SiC polytypes is $J_1 \cong -2J_2$ (for $n > 2$, $J_n \ll J_1, J_2$) which is the 3C, 4H, 6H degeneracy point. The interlayer interaction parameter points obtained from the first-principles calculations of [4–6] appear away from the

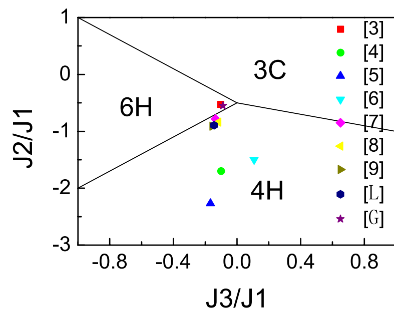

Figure 1. Phase diagram of the ground states. The ratios J_3/J_1 and J_2/J_1 are coordinates. The results of [3–9] are marked with [3], [4], . . . , [9], respectively. Our results obtained with the DFT-LDA and DFT-GGA are marked with [L] and [G], respectively.

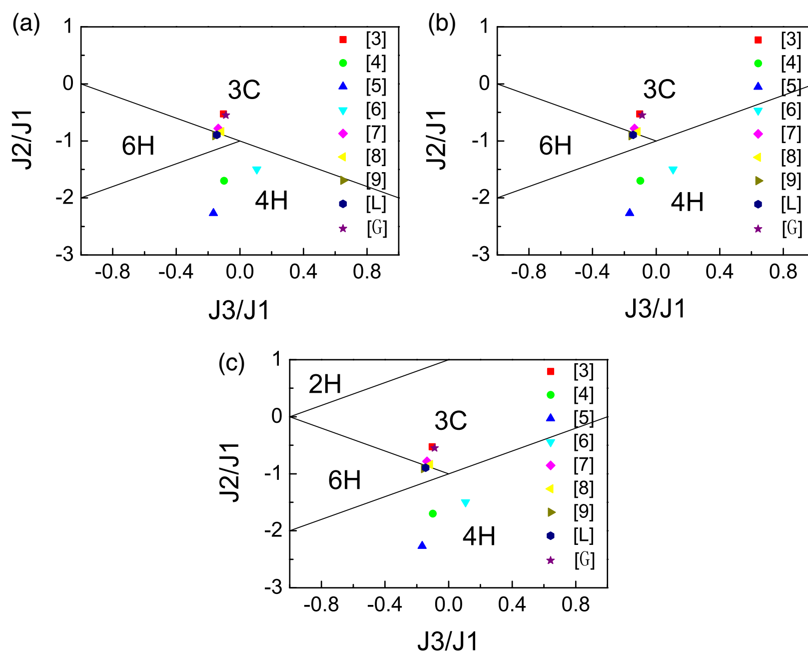

Figure 2. The layered growth phase diagrams of epitaxial growth processes when the rearrangement of atoms in one surface bilayer is allowed. The stability regions of the polytypes are indicated. The results of [3–9] are marked with [3], [4], . . . , [9], respectively. Our results obtained with the DFT-LDA and DFT-GGA are marked with [L] and [G], respectively. (a) The substrate structure is $(\bar{1}\bar{1}\bar{1})$; (b) the substrate structures are $(\bar{1}\bar{1}1)$ or $(1\bar{1}\bar{1})$; (c) the substrate structure is $(\bar{1}1\bar{1})$.

triple point, and could not explain the origin of the polytypism in SiC. However, the interlayer interaction parameter point obtained from our DFT-GGA result is very close to the triple point. The interlayer interaction parameter points obtained from our first-principles results and those of [3, 7–9] are close to the boundary of the 4H and 6H phases, which confirms that the total energy difference of 4H-SiC and 6H-SiC is very small.

The layered growth phase diagrams for epitaxial growth processes when the rearrangement of atoms in one surface Si–C bilayer is allowed to orient the surface Si–C bilayer into its most energetically favourable stacking orientation are plotted in figure 2. The phase diagrams for

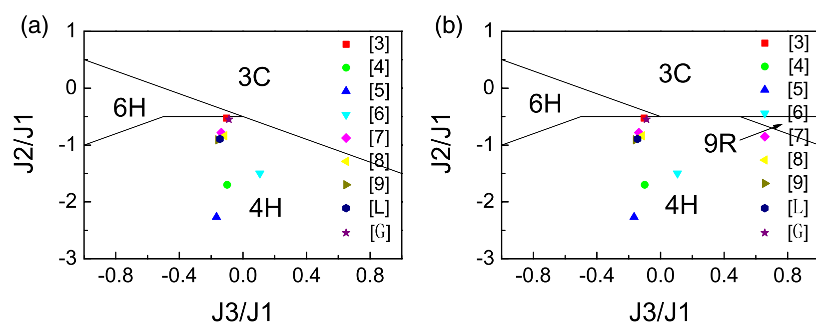

Figure 3. The layered growth phase diagrams of epitaxial growth processes when the rearrangement of atoms in two surface bilayers is allowed. The stability regions of the polytypes are indicated. The results of [3–9] are marked with [3], [4], . . . , [9], respectively. Our results obtained with the DFT-LDA and DFT-GGA are marked with [L] and [G], respectively. (a) The substrate structure is $(\bar{1}\bar{1}\bar{1})$; (b) the substrate structures are $(\bar{1}\bar{1}1)$, $(1\bar{1}\bar{1})$ or $(\bar{1}1\bar{1})$.

the substrate structures $(\bar{1}\bar{1}1)$ and $(1\bar{1}\bar{1})$ are the same, so we show them in one figure. It can be seen that figures 2(a) and (b) are the same in the region where $J_3/J_1 \leqslant 0$. When $J_3/J_1 > 0$, the parameter region for the 3C-SiC phase is much larger in figure 2(a). The difference between figures 2(c) and (b) is that there is a 2H-SiC phase region in figure 2(c). Figures 2(a)–(c) are the same in the region of $J_3/J_1 \leqslant 0$ and $J_2/J_1 \leqslant 0$. We have indicated interlayer interaction parameter points obtained from our first-principles results and those of [3–9] with different symbols in the phase diagrams. It can be seen that our DFT-GGA result and those of [3, 7, 8] lie in the area of the 3C-SiC phase, our DFT-LDA result and that of [9] lie in the region of the 6H-SiC phase and the parameter points from [4–6] lie in the region of the 4H-SiC phase. Our DFT-LDA result and those of [4–6, 9] cannot explain the experimental phenomenon that silicon carbide appears to prefer to grow in the 3C-SiC phase, more than in any other, in spite of the fact that the 3C-SiC phase is not the lowest-energy structure. Our DFT-GGA result and those of [3, 7, 8] are in agreement with that of Heine [12]. For silicon carbide (SiC), the results of simulation show that the resulting structures do not depend on the substrate structures.

The layered growth phase diagrams for epitaxial growth processes when the arrangement of atoms in two surface Si–C bilayers is allowed to orient the two surface Si–C bilayers into their most energetically favourable stacking orientations are plotted in figure 3. The phase diagrams for the substrate structures $(\bar{1}\bar{1}1)$, $(1\bar{1}\bar{1})$ and $(\bar{1}1\bar{1})$ are the same, so we show them in one figure. It can be seen that in the region where $J_3/J_1 > 0$, figures 3(a) and (b) are different. The parameter region for the 3C-SiC phase is much larger in figures 3(a) and (b) and has a region for the 9R-SiC phase. We have indicated interlayer interaction parameter points obtained from our first-principles results and those of [3–9] with different symbols in the phase diagrams. It can be seen that they all lie in the region of the 4H-SiC phase for all the substrate structures.

The layered growth phase diagrams for epitaxial growth processes when the arrangement of atoms in three surface Si–C bilayers is allowed to orient the three surface Si–C bilayers into their most energetically favourable stacking orientations are plotted in figure 4. The phase diagrams for the substrate structures $(\bar{1}\bar{1}1)$, $(1\bar{1}\bar{1})$ and $(\bar{1}1\bar{1})$ are the same, so we show them in one figure. It can be seen that in the region where $J_3/J_1 > 0$, figures 4(a) and (b) are different. The parameter region for the 3C-SiC phase is much larger in figures 4(a) and (b) and has a region for the 9R-SiC phase. We have indicated interlayer interaction parameter points obtained from our first-principles results and those of [3–9] with different symbols in

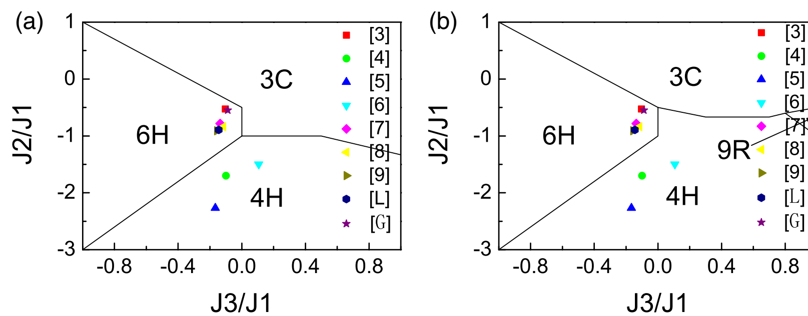

Figure 4. The layered growth phase diagrams of epitaxial growth processes when the rearrangement of atoms in three surface bilayers is allowed. The stability regions of the polytypes are indicated. The results of [3–9] are marked with [3], [4], . . . , [9], respectively. Our results obtained with the DFT-LDA and DFT-GGA are marked with [L] and [G], respectively. (a) The substrate structure is $(\bar{1}\bar{1}\bar{1})$; (b) the substrate structures are $(\bar{1}\bar{1}1)$, $(1\bar{1}\bar{1})$ or $(\bar{1}1\bar{1})$.

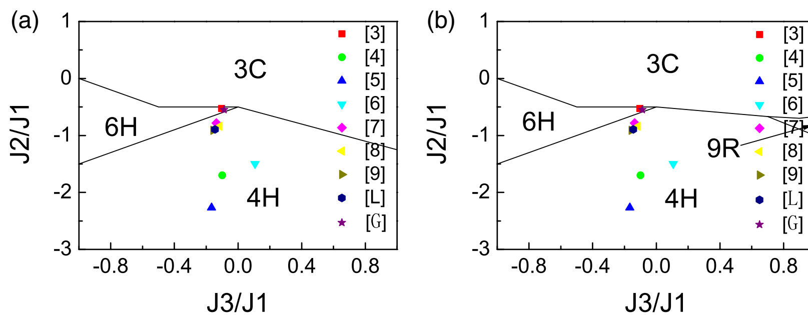

Figure 5. The layered growth phase diagrams of epitaxial growth processes when the rearrangement of atoms in four surface bilayers is allowed. The stability regions of the polytypes are indicated. The results of [3–9] are marked with [3], [4], . . . , [9], respectively. Our results obtained with the DFT-LDA and DFT-GGA are marked with [L] and [G], respectively. (a) The substrate structure is $(\bar{1}\bar{1}\bar{1})$; (b) the substrate structures are $(\bar{1}\bar{1}1)$, $(1\bar{1}\bar{1})$ or $(\bar{1}1\bar{1})$

the phase diagrams. It can be seen that the parameter points from [4–6] lie in the region of the 4H-SiC phase while our first-principles results and those of [3, 7–9] lie in the region of the 6H-SiC phase. The results do not depend on the substrate structures.

The layered growth phase diagrams for epitaxial growth processes when the arrangement of atoms in four surface Si–C bilayers is allowed to orient the four surface Si–C bilayers into their most energetically favourable stacking orientations are plotted in figure 5. The phase diagrams for the substrate structures $(\bar{1}\bar{1}1)$, $(1\bar{1}\bar{1})$ and $(\bar{1}1\bar{1})$ are the same, so we show them in one figure. It can be seen that in the region where $J_3/J_1 > 0$, figures 5(a) and (b) are different. The parameter region for the 3C-SiC phase is much larger in figures 5(a) and (b) and has a region for the 9R-SiC phase. We have indicated interlayer interaction parameter points obtained from our first-principles results and those of [3–9] with different symbols in the phase diagrams. It can be seen that the parameter points from our DFT-LDA result and those of [4–9] lie in the region of the 4H-SiC phase while our DFT-GGA result and that of [3] lie in the region of the 6H-SiC phase. The results do not depend on the substrate structures.

The layered growth phase diagrams for epitaxial growth processes when the arrangement of atoms in five surface Si–C bilayers is allowed to orient the five surface Si–C bilayers into their most energetically favourable stacking orientations are plotted in figure 6. The phase

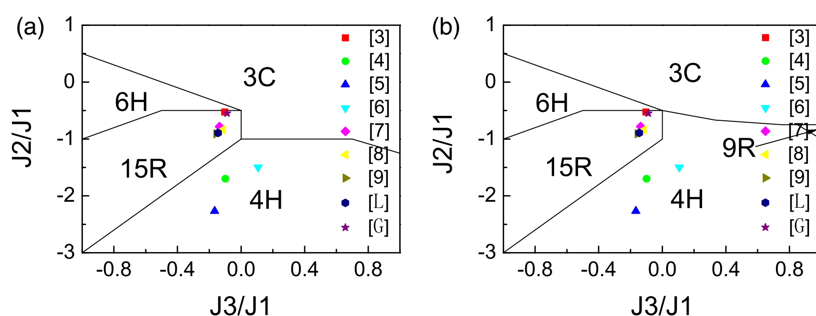

Figure 6. The layered growth phase diagrams of epitaxial growth processes when the rearrangement of atoms in five surface bilayers is allowed. The stability regions of the polytypes are indicated. The results of [3–9] are marked with [3], [4], . . . , [9], respectively. Our results obtained with the DFT-LDA and DFT-GGA are marked with [L] and [G], respectively. (a) The substrate structure is $(\bar{1}\bar{1}\bar{1})$; (b) the substrate structures are $(\bar{1}\bar{1}1)$, $(1\bar{1}\bar{1})$ or $(\bar{1}1\bar{1})$.

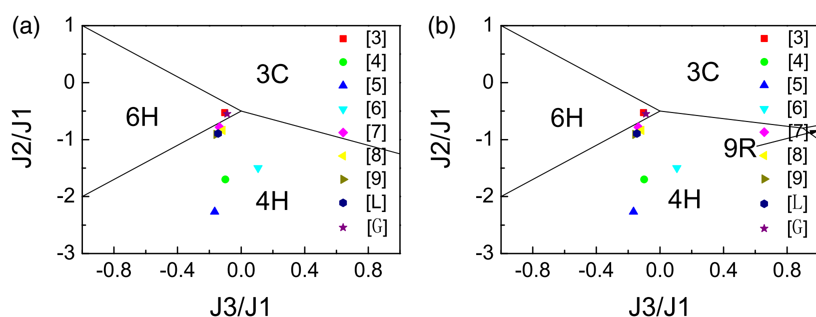

Figure 7. The layered growth phase diagrams of epitaxial growth processes when the rearrangement of atoms in six surface bilayers is allowed. The stability regions of the polytypes are indicated. The results of [3–9] are marked with [3], [4], . . . , [9], respectively. Our results obtained with the DFT-LDA and DFT-GGA are marked with [L] and [G], respectively. (a) The substrate structure is $(\bar{1}\bar{1}\bar{1})$; (b) the substrate structures are $(\bar{1}\bar{1}1)$, $(1\bar{1}\bar{1})$ or $(\bar{1}1\bar{1})$.

diagrams for the substrate structures $(\bar{1}\bar{1}1)$, $(1\bar{1}\bar{1})$ and $(\bar{1}1\bar{1})$ are the same, so we show them in one figure. It can be seen that in the region where $J_3/J_1 > 0$, figures 6(a) and (b) are different. The parameter region for the 3C-SiC phase is much larger in figures 6(a) and (b) and has a region for the 9R-SiC phase. We have indicated interlayer interaction parameter points obtained from our first-principles results and those of [3–9] with different symbols in the phase diagrams. It can be seen that our first-principles results and those of [3, 7–9] lie in the region of the 15R-SiC phase while the parameter points from [4–6] lie in the region of the 4H-SiC phase. The results do not depend on the substrate structures.

The layered growth phase diagrams for epitaxial growth processes when the arrangement of atoms in six surface Si–C bilayers is allowed to orient the six surface Si–C bilayers into their most energetically favourable stacking orientations are plotted in figure 7. The phase diagrams for the substrate structures $(\bar{1}\bar{1}1)$, $(1\bar{1}\bar{1})$ and $(\bar{1}1\bar{1})$ are the same, so we show them in one figure. It can be seen that in the region where $J_3/J_1 \leqslant 0$, figures 7(a) and (b) are the same as the phase diagram of the ground states (figure 1), which shows that the resulting phases of simulation become closer to the ground states as the number of surface Si–C bilayers in which the rearrangement of atoms is allowed increases. We have indicated interlayer interaction parameter points obtained from our first-principles results and those of [3–9] with different

symbols in the phase diagrams. It can be seen that the parameter points from our DFT-LDA result and those of [4–9] lie in the region of the 4H-SiC phase while our DFT-GGA result and that of [3] lie in the region of the 6H-SiC phase for all the substrate structures.

4. Conclusion

In summary, our first-principles calculations show that the total energies of SiC polytypes are in the order $E_{6H} < E_{4H} < E_{3C} < E_{2H}$, from the results obtained with the DFT-GGA and $E_{4H} < E_{6H} < E_{3C} < E_{2H}$ from the results obtained with the DFT-LDA, respectively. Since the first-principles calculation with the DFT-GGA could generally give a more precise total energy than that with the DFT-LDA, we prefer to use the results obtained with the DFT-GGA to discuss the growth of SiC. From the layered growth phase diagrams, it can be seen that when the rearrangement of atoms in one surface Si–C bilayer is allowed, the 3C-SiC structure is formed, in agreement with Heine [12]. When the rearrangement of atoms in two surface Si–C bilayers is allowed, the 4H-SiC structure is formed. When the rearrangement of atoms in more than two surface Si–C bilayers, excepting the case of five surface Si–C bilayers, is allowed, the 6H-SiC structure is formed. As the temperature of the epitaxial growth process increases or the annealing process becomes slower, the number of surface Si–C bilayers where the rearrangement of atoms is allowed increases. Thus the ground state is easier to grow at high temperatures. Our results show that the 6H-SiC phase is the ground state phase with the lowest total energy. This is in agreement with experiments [2, 33, 46], which indicate that 6H-SiC is the stable phase at high temperatures and probably 4H-SiC is stable at low temperatures. Polytypic transformation of 4H-SiC into 6H-SiC has been observed experimentally [47, 48]. When the rearrangement of atoms in five surface Si–C bilayers is allowed, the 15R-SiC phase is formed, which explains the experimental phenomenon that 15R-SiC can be formed in spite of the fact that this is never the stable structure [49, 50]. Thus we conclude that the 3C-SiC phase would grow epitaxially at low temperature, 4H-SiC would grow epitaxially at intermediate temperature and 6H-SiC or 15R-SiC would grow epitaxially at higher temperature.

Acknowledgments

This research was supported by the National Natural Science Foundation of China under Grant No 10274036 and the National Basic Research Program of China under Grant No G2000067107.

References

[1] Casady J B and Johnson R W 1996 *Solid-State Electron.* **39** 1409
Carter C H and Tsvetkov V F 1999 *Mater. Sci. Eng.* B **61/62** 1
[2] Jepps N W and Page T F 1983 *Prog. Cryst. Growth Charact.* **7** 259
[3] Cheng C, Needs R J and Heine V 1988 *J. Phys. C: Solid State Phys.* **21** 1049
[4] Park C H, Cheong B H, Lee K H and Chang K J 1994 *Phys. Rev.* B **49** 4485
[5] Käckell P, Wenzien B and Bechstedt F 1994 *Phys. Rev.* B **50** 17037
[6] Karch K, Wellenhofer G, Pavone P, Rössler U and Strauchin D 1995 *Proc. 22nd Int. Conf. on the Physics of Semiconductors* (Singapore: World Scientific) p 401
[7] Rutter M J and Heine V 1997 *J. Phys.: Condens. Matter* **9** 8213
[8] Limpijumnong S and Lambrecht W R L 1998 *Phys. Rev.* B **57** 12017
[9] Lindefeilt U, Iwata H, Öberg S and Briddon P R 2003 *Phys. Rev.* B **67** 155204
[10] Cheng C, Heine V and Needs R J 1990 *J. Phys.: Condens. Matter* **2** 5115

[11] Bechstedt F, Käckell P, Zywietz A, Karch K, Adolph B, Tenelsen K and Furthmüller J 1997 *Phys. Status Solidi* B **202** 35
[12] Heine V, Cheng V and Needs R J 1991 *J. Am. Ceram. Soc.* **74** 2630
[13] Heine V, Cheng V, Engel G E and Needs R J 1992 *Wide Band Gap Semiconductors* (*MRS Symp. Proc. No.* 242) (Pittsburgh, PA: Materials Research Society) p 507
[14] Heine V, Cheng C and Needs R J 1992 *Mater. Sci. Eng.* B **11** 55
[15] Cheng C, Heine V and Jones I L 1990 *J. Phys.: Condens. Matter* **2** 5097
[16] Zywietz A, Karch K and Bechstedt F 1996 *Phys. Rev.* B **54** 1791
[17] Grossner U, Fissel A, Furthmüller J, Richter W and Bechstedt F 2001 *Mater. Sci. Forum.* **353–356** 211
[18] Fissel A, Schröter B, Kaiser U and Richter W 2000 *Appl. Phys. Lett.* **77** 2418
[19] Fissel A, Schröter B, Kaiser U, Richter W and Bechstedt F 2001 *Appl. Surf. Sci.* **184** 37
[20] Kuroda N, Shibahara K, Yoo W S, Nishino S and Matsunami H 1987 *Extended Abstracts of the 19th Conf. on Solid State Devices and Materials (Tokyo, Japan)* p 227
[21] Kong H S, Kim H J, Edmond J A, Palmour J W, Ryu J, Carter C H Jr, Glass J T and Davis R F 1987 *Mater. Res. Soc. Symp. Proc.* **97** 233
[22] Shibahara K, Kuroda N, Nishino S and Matsunami H 1987 *Japan. J. Appl. Phys.* 2 **26** L1815
[23] Franks F C 1951 *Phil. Mag.* **43** 1014
[24] Powell J A and Will H A 1972 *J. Appl. Phys.* **43** 1400
[25] Kimoto T and Matsunami H 1994 *J. Appl. Phys.* **76** 7322
[26] Jennings V J, Sommer A and Chang H 1966 *J. Electrochem. Soc.* **113** 728
[27] Von Muench W and Phaffeneder I 1976 *Thin Solid Films* **31** 39
[28] Tairov Yu M and lhvetkov V F 1981 *J. Cryst. Growth* **52** 146
[29] Fissel A, Kaiser U, Ducke E, Schröter B and Richter W 1995 *J. Cryst. Growth* **154** 72
[30] Fissel A, Schröter B and Richter W 1999 *Solid State Phys.* **38** 87
[31] Fissel A, Pfennighaus K, Kaiser U, Schröter B and Richter W 1999 *J. Electron. Mater.* **28** 206
[32] Fissel A, Kaiser U, Kräusslich J, Pfennighaus K, Schröter B, Schulze J and Richter W 1999 *Mater. Sci. Eng.* B **61/62** 139
[33] Ness N and Page T F 1986 *Bull. Mineral.* **109** 151
[34] Nutt S R and Wawner F E 1985 *J. Mater. Sci.* **20** 1953
[35] Yang J, Nishino S, Powell J A and Pirouz P 1994 *Silicon Carbide and Related Materials* (*Inst. Phys. Conf. Ser. 137*) (Bristol: Institute of Physics Publishing) p 25
[36] Nishino K, Kimoto T and Matsunami H 1994 *Silicon Carbide and Related Materials* (*Inst. Phys. Conf. Ser. 137*) (Bristol: Institute of Physics Publishing) p 33
[37] Von Boehm J and Bak P 1979 *Phys. Rev. Lett.* **42** 122
[38] Kresse G and Hafner J 1993 *Phys. Rev.* B **47** 558
Kresse G and Hafner J 1994 *Phys. Rev.* B **49** 14251
Kresse G and Furthmüller J 1996 *Comput. Mater. Sci.* **6** 15
Kresse G and Furthmüller J 1996 *Phys. Rev.* B **54** 11169
[39] Kresse G and Joubert D 1999 *Phys. Rev.* B **59** 1758
[40] Perdew J P, Chevary J A, Vosko S H, Jackson K A, Pederson M R, Singh D J and Fiolhais C 1992 *Phys. Rev.* B **46** 6671
[41] Ceperley D M and Alder B J 1980 *Phys. Rev. Lett.* **45** 566
[42] Perdew J P and Zunger A 1981 *Phys. Rev.* B **23** 5048
[43] *Properties of Silicon Carbide* 1995 (*EMIS Datareviews Series No* 13) (London: Institution of Electrical Engineers)
[44] Bauer A, Kräusslich J, Dressler L, Kuschnerus P, Wolf J, Goetz K, Käckell P, Furthmüller J and Bechstedt F 1998 *Phys. Rev.* B **57** 2647
[45] Adamsky R F and Merz K M 1959 *Z. Kristallogr.* **111** 350
[46] Pandey D 1989 *Phase Transit.* **16/17** 247
[47] Bootsma G A 1971 *J. Cryst. Growth* **8** 347
[48] *Current Topics in Materials Science* 1982 vol 9 (New York: North-Holland) p 468
[49] Stein R A and Lanig P 1993 *J. Cryst. Growth* **131** 71
[50] Semmelroth K, Schulze N and Pensl G 2004 *J. Phys.: Condens. Matter* **16** S1579